Title

On the use of surrogate-based modeling for the numerical analysis of Low Impact Development techniques

Authors

Brunetti, Giuseppe
Šimůnek, Jirka
Turco, Michele
et al.

Research papers

On the use of surrogate-based modeling for the numerical analysis of Low Impact Development techniques

CrossMark

Giuseppe Brunetti [a],[*], Jirka Šimůnek [b], Michele Turco [a], Patrizia Piro [a]

[a] Department of Civil Engineering, University of Calabria, Rende, CS 87036, Italy
[b] Department of Environmental Sciences, University of California, Riverside, Riverside, CA 92521, USA

ABSTRACT

Mechanistic models have proven to be accurate tools for the numerical analysis of the hydraulic behavior of Low Impact Development (LIDs) techniques. However, their widespread adoption has been limited by their computational cost. In this view, surrogate modeling is focused on developing and using a computationally inexpensive *surrogate* of the *original* model. While having been previously applied to various water-related and environmental modeling problems, no studies have used surrogate models for the analysis of LIDs. The aim of this research thus was to investigate the benefit of surrogate-based modeling in the numerical analysis of LIDs. The kriging technique was used to approximate the deterministic response of the widely used mechanistic model HYDRUS-2D, which was employed to simulate the variably-saturated hydraulic behavior of a contained stormwater filter. The Nash-Sutcliffe efficiency (*NSE*) index was used to compare the simulated and measured outflows and as the variable of interest for the construction of the response surface. The validated kriging model was first used to carry out a Global Sensitivity Analysis of the unknown soil hydraulic parameters of the filter layer, revealing that only the shape parameter α and the saturated hydraulic conductivity K_s significantly affected the model response. Next, the Particle Swarm Optimization algorithm was used to estimate their values. The *NSE* value of 0.85 indicated a good accuracy of estimated parameters. Finally, the calibrated model was validated against an independent set of measured outflows with a *NSE* value of 0.8, which again corroborated the reliability of the surrogate-based optimized parameters.

© 2017 Elsevier B.V. All rights reserved.

1. Introduction

During the last few decades, stormwater management has become a major component of the prevention of floods in urban areas and for the preservation of water resources. An increase of impervious surfaces, connected with demographic growth, has altered the natural hydrological cycle by reducing the infiltration and evaporation capacity of urban catchments while also increasing surface runoff. In their report, the Organization for Economic Co-operation and Development (OECD) (2013) identified an expected increase in flash and urban floods in large parts of Europe as one of the major issues for the future.

In this context, urban drainage systems play a fundamental role in improving the resilience of cities. In recent years, an innovative approach to land development known as a Low Impact Development (LID) has gained increasing popularity. A LID is a 'green' approach to storm water management that seeks to mimic the nat-

ural hydrology of a site using decentralized micro-scale control measures (Coffman, 2002). LID practices consist of bioretention cells, infiltration wells/trenches, storm water wetlands, wet ponds, level spreaders, permeable pavements, swales, green roofs, vegetated filter/buffer strips, sand and gravel filters, smaller culverts, and water harvesting systems. Several studies have evaluated the benefits of LIDs. For example, Newcomer et al. (2014) used a numerical model to demonstrate the benefits of LIDs, and an infiltration trench in particular, on recharge and local groundwater resources for future climate scenarios. In another paper, Berardi et al. (2014) demonstrated how green roofs may contribute to the development of more sustainable buildings and cities. Green Roofs (GR) were able to significantly reduce peak rates of storm water runoff (Getter et al., 2007) and retain rainfall volumes with retention efficiencies ranging from 40% to 80% (Bengtsson et al., 2004). Permeable pavements offered great advantages in terms of runoff reduction (Carbone et al., 2014; Collins et al., 2008), water retention, and water quality (Brattebo and Booth, 2003). Even though the results of available studies are encouraging, more

* Corresponding author.
   E-mail address: giusep.bru@gmail.com (G. Brunetti).

research is needed to precisely assess the impact of LIDs on the hydrological cycle.

As pointed out by several authors (e.g., Elliot and Trowsdale, 2007; Wong et al., 2006), there is a strong demand for predictive models that can be applied across a range of locations and conditions to predict the general performance of a range of stormwater treatment measures. In recent years, researchers have focused their attention on applying and developing empirical, conceptual, and physically-based models for LIDs analysis. In their review article, Li and Babcock (2014) reported that there were >600 papers published worldwide involving green roofs, with a significant portion of them related to modeling. Several studies demonstrated that physically-based models can provide a rigorous description of various relevant processes such as variably-saturated water flow, evaporation and root water uptake, solute transport, heat transport, and carbon sequestration. Brunetti et al. (2016a, 2016b) used a mechanistic model, HYDRUS-3D (Šimůnek et al., 2016; Šimůnek et al., 2008), to analyze an extensive green roof in a Mediterranean climate. The model, previously validated against field scale measurements, was used to investigate the hydraulic response of a green roof to single precipitation events and its hydrological behavior during a two-month period. Metselaar (2012) used the SWAP model (van Dam et al., 2008) to simulate the one-dimensional water balance of a substrate layer on a flat roof with plants. Li and Babcock (2015) used HYDRUS-2D to model the hydrologic response of a pilot green roof system. The model was calibrated using water content measurements obtained with TDR (Time Domain Reflectometer) sensors. The calibrated model was then used to simulate the potentially beneficial effects of irrigation management on the reduction of runoff volumes. The VFSMOD model (Munoz-Carpena and Parsons, 2004) was extensively used for the analysis of the hydraulic behavior and solute transport of vegetated filter strips (Abu-Zreig et al., 2001; Dosskey et al., 2002).

However, physically-based modeling often involves highly non-linear, partial, differential equations that are solved using various numerical approximation methods, requiring a high computational cost. Moreover, a comprehensive simulation framework includes model calibration, sensitivity analysis, and uncertainty quantification aimed at enhancing confidence in the model and its ability to describe real world systems. These tasks require running the simulation model hundreds or thousands of times and thus the computational cost exponentially increases.

Surrogate modeling focuses on developing and using a computationally inexpensive *surrogate* of the *original* model. The main aim is to approximate the response of an original simulation model, which is typically computationally intensive, for various quantities of interest (Razavi et al., 2012). Surrogate models have been widely applied in various water-related and environmental modeling problems. Khu and Werner (2003) used artificial neural networks (ANN) in conjunction with genetic algorithms (GA) to reduce the computational budget required in the uncertainty quantification framework of the rainfall-runoff model SWMM. The GA was first used to identify the areas of higher importance in the parameter space and ANNs were then used to approximate the response surface in these areas (Khu and Werner, 2003). Borgonovo et al. (2012) tested a surrogate model for the estimation of the sensitivity indices of an environmental model. Zhang et al. (2009) evaluated ANN and Support Vector Machine (SVM) for approximating the Soil and Water Assessment Tool (SWAT) model in two watersheds. Keating et al. (2010) used a surrogate model to carry out a comparison between the null-space Monte Carlo sampling (NSMC) and the DiffeRential Evolution Adaptive Metropolis (DREAM) algorithm for parameter estimation and uncertainty quantification. In another study, Laloy et al. (2013) used Polynomial Chaos Expansion (PCE) to emulate the output of a large-scale flow model. The surrogate

model was used in a Bayesian analysis framework to derive the posterior distribution of different parameters. In their study, Younes et al. (2013) used a surrogate model to estimate three soil hydraulic parameters from a drainage experiment. In particular, PCE was used to run a Monte Carlo Markov Chain (MCMC) analysis. However, although the widespread diffusion of surrogate modeling tools could drastically reduce computational budgets, their use for physically-based modeling of LIDs is still unexploited.

The primary objective of this paper is to investigate the suitability of surrogate modeling for the numerical analysis of LIDs techniques by analyzing data from a real case study. The mechanistic model HYDRUS-2D is first used to simulate the hydraulic behavior of a Stormwater Filter (SF) at the University of Calabria, Italy. The surrogate model, based on kriging, is then used to carry out a Global Sensitivity Analysis (GSA) and a Global Optimization of soil hydraulic parameters. The use of a surrogate model for the sensitivity analysis of model outputs to soil hydraulic properties represents a new application of this technique that can provide a significant contribution in this field.

The problem is addressed in the following way. First, the evaporation method is used to measure the soil hydraulic properties of the vegetated substrate above the gravel filter, for which the hydraulic properties were unknown. The measured soil hydraulic properties of the vegetated substrate and the selected ranges of parameters of the filter layer are then used in HYDRUS-2D to set up the model. A Latin Hypercube Sampling (LHS) plan is used to build a first trial of the surrogate model. Before continuing with the other tasks, the surrogate model is validated and improved by using specific infill criteria. Once validated, the surrogate model is first used for the GSA based on Sobol's method to compute the sensitivity measures, and then for the inverse parameter estimation carried out using the Particle Swarm Optimization (PSO) algorithm. Finally, estimated parameters are used in the original mechanistic model for the validation purpose.

2. Materials and methods

2.1. Stormwater filter and site description

The University of Calabria is located in the south of Italy, in the vicinity of Cosenza (39°18′ N 16°15′ E). The climate is Mediterranean with a mean annual temperature of 15.5 °C and average annual precipitation of 881.2 mm. The stormwater filter (SF) has a surface area of 125 m^2, an average slope of 2%, and a total profile depth of 0.75 m. Fig. 1 shows a schematic of the SF.

The filter layer is covered by a vegetated soil substrate with a measured bulk density of 1.59 g/cm^3. A high permeability geotextile with a fiber area weight of 60 g/m^2 is placed at the interface between the soil substrate and the filter layer to prevent fine particles from migrating into the underlying layer. The filter layer is composed of a gravelly material characterized by a high permeability. An impervious membrane is placed at the bottom of the profile to prevent water from percolating into deeper horizons.

The SF is used to treat stormwater runoff from the adjoining impervious parking lot, which is characterized by an area of 220 m^2. Stormwater runoff from the parking lot is first conveyed into a manhole and then to an instrumented channel where the flow rate is measured by a flux meter composed of a rectangular, sharp crested weir coupled with a pressure transducer. The pressure transducer (Ge Druck PTX1830) measures the water level inside the channel and has a range of measurements of 75 cm with an accuracy of 0.1% of the full scale. The pressure transducer was calibrated in the laboratory using a hydrostatic water column, linking the electric current intensity with the water level inside the
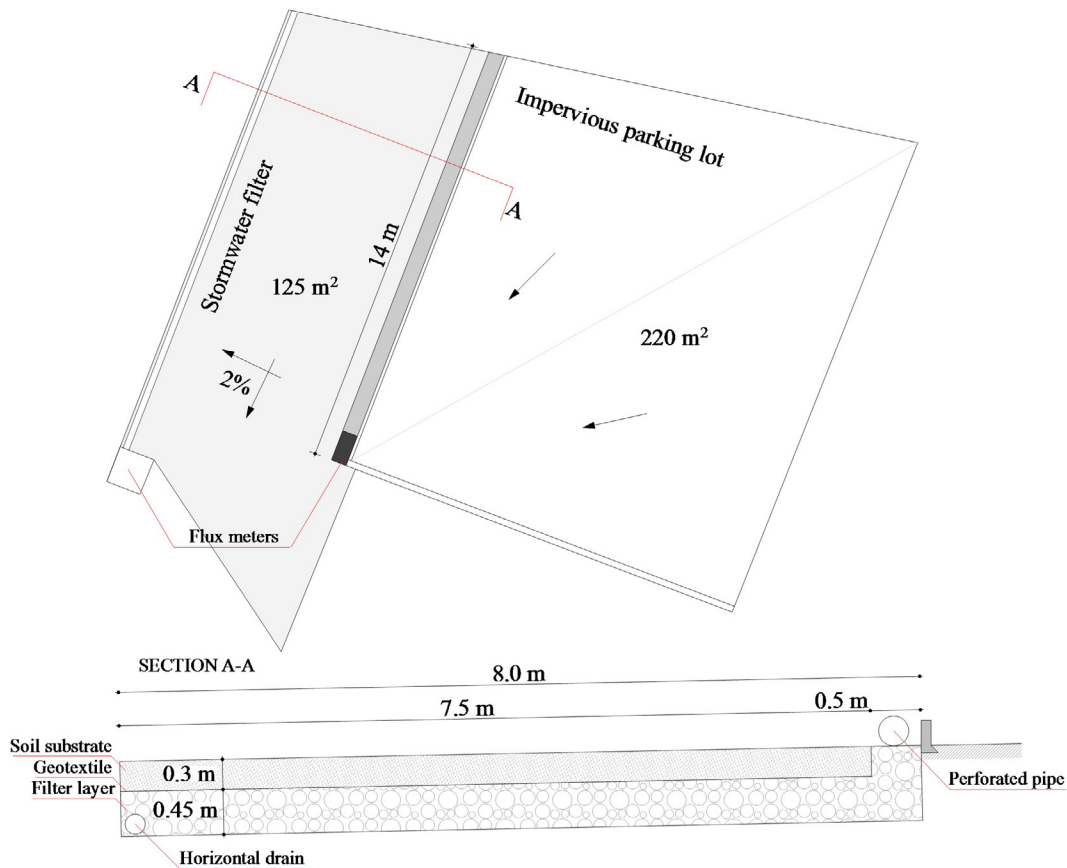
Fig. 1. A schematic of the experimental site (top) and a typical cross-section (bottom) of the stormwater filter.

column. An exponential head-discharge equation for the flux meter was obtained by fitting the experimental data.

Measured runoff is next conveyed into a 14 m long, horizontal perforated pipe where it is distributed on the top of the filter layer (Fig. 1). As shown in Fig. 1, the soil substrate is not used to treat stormwater runoff, which is directly routed into the filter, but only to increase the retention and evapotranspiration capacity of the system itself. The baseflow is collected in a horizontal drain, which consists of a perforated PVC pipe, and is conducted to a manhole for quantity and quality measurements. A second flux meter, composed of a PVC pipe with a sharp-crested weir and a pressure transducer, measures the flow rate. Runoff and baseflow data were acquired with a time resolution of one minute and stored in a SQL database. No measurements of pressure heads or volumetric water contents inside of the filter were taken.

A weather station located directly at the site measures precipitation, wind velocity and direction, air humidity, air temperature, atmospheric pressure, and global solar radiation. Rain data are measured using a tipping bucket rain gauge with a resolution of 0.254 mm and an acquisition frequency of one minute. Climatic data are acquired with a frequency of five minutes. Data are processed and stored in the SQL database.

Two month-long data sets were selected for the analysis (Fig. 2). The first data set, which started on 2014-01-15 and ended on 2014-02-15, was used for obtaining the surrogate model. The second data set, which started on 2014-03-01 and ended on 2014-03-31, was used for model validation. The precipitation totals for the first and second data sets were 274 and 174 mm, respectively. The second data set was selected because it had significantly different meteorological dynamics than during the first period. The optimization set is characterized by multiple rain events with few dry

periods. The validation set has fewer rain events, which are concentrated at the beginning and end of the time period and separated by a relatively long dry period.

Hourly reference evapotranspiration was calculated using the Penman-Monteith equation (Allen et al., 1998). Considering that vegetation mainly consisted of herbaceous plants, an average value of albedo of 0.23 was assumed in calculations of net short-wave radiation (Breshears et al., 1997).

2.2. Evaporation method and parameter estimation

2.3.1. Evaporation method

Modeling of water flow in unsaturated soils by means of the Richards equation requires knowledge of the water retention function, $\theta(h)$, and the hydraulic conductivity function, $K(h)$, for each soil layer of the SF, where θ is the volumetric water content $[L^3 L^{-3}]$, h is the pressure head $[L]$, and K is the hydraulic conductivity $[LT^{-1}]$. In order to reduce the dimensionality of the optimization problem, the soil hydraulic properties of the soil substrate were measured in the laboratory using a simplified evaporation method with an extended measurement range (down to -9000 cm), as proposed by Schindler et al. (2010a, 2010b). For a detailed description of the modified evaporation method, please refer to Schindler et al. (2010a, 2010b).

Peters and Durner (2008) conducted a comprehensive error analysis of the simplified evaporation method and concluded that it is a fast, accurate, and reliable method to determine soil hydraulic properties in the measured pressure head range, and that the linearization hypothesis introduced by Schindler (1980) causes only small errors. The above cited method has already been used in the LIDs analysis for the determination of the unsaturated soil
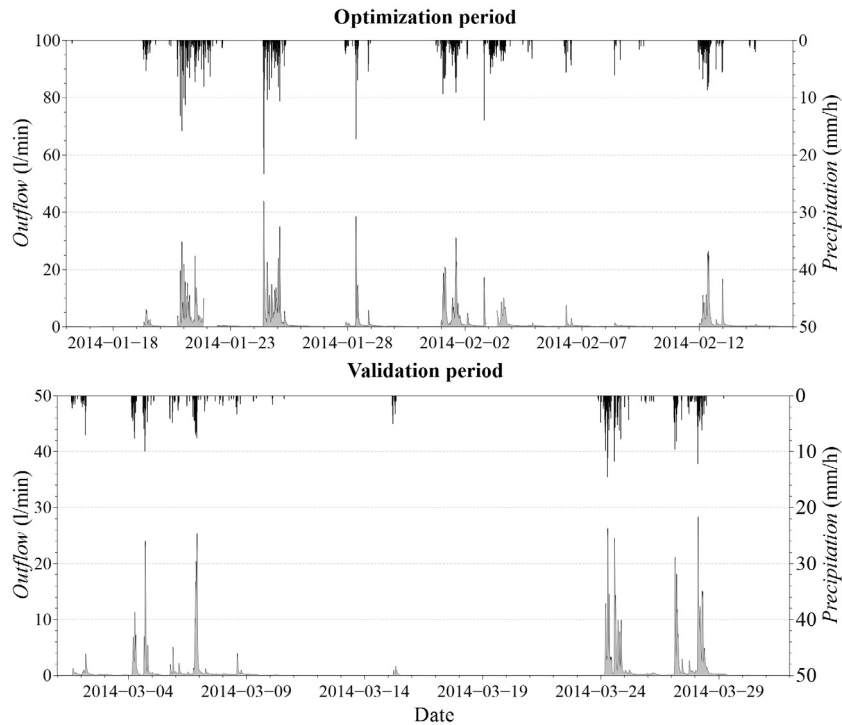
Fig. 2. Precipitation (black line) and subsurface flow (grey line) for the optimization (top) and validation (bottom) periods, respectively.

hydraulic properties of a green roof substrate (Brunetti et al., 2016a). In that study, the measured soil hydraulic properties were used in HYDRUS-3D to simulate the hydraulic behavior of a green roof and validated by providing optimal correspondence between simulated and measured outflows. The simplified evaporation method was similarly used in this study for the determination of the unsaturated hydraulic properties of the soil substrate. For a complete description of the system, please refer to UMS GmbH (2015).

The soil for the laboratory analysis was directly sampled from the SF using a stainless-steel sampling ring with a volume of 250 ml. The soil sample was saturated from the bottom before starting the evaporation test. The measurement unit and tensiometers were degassed using a vacuum pump, in order to reduce the potential nucleation sites in the demineralized water. Since Peters and Durner (2008) suggested a reading interval for structured soils of less than 0.1 day, the reading interval was set to 20 min in order to have high resolution measurements. At the end of the experiment, the sample was placed in an oven at 105 °C for 24 h, and then the dry weight was measured.

2.4. Parameter estimation

The numerical optimization procedure, HYPROP-FIT (Pertassek et al., 2015), was used to simultaneously fit retention and hydraulic conductivity functions to experimental data obtained using the evaporation method. Fitting was accomplished using a non-linear optimization algorithm that minimizes the sum of weighted squared residuals between model predictions and measurements. The software uses the Shuffled Complex Evolution (SCE) algorithm proposed by Duan et al. (1992), which is a global parameter estimation algorithm. The goodness-of-fit was evaluated in terms of the Root Mean Square Error (RMSE), while the Akaike information criterion (AIC) (Hu, 1987) was used to choose between different hydraulic conductivity functions. The software also provides 95%

confidence intervals to assess the uncertainty in parameter estimation. In order to calculate the parameter uncertainties a linear approximation of the covariance matrix for each estimated parameter is calculated. The confidence interval for the i-th parameter is then computed by combining the covariance matrix and the upper $a/2$ quantile of the Students t-distribution, where a is set to 0.05 for the computation of the 95% confidence intervals.

2.5. Modeling theory

2.5.1. Water flow and root water uptake
The HYDRUS-2D software (Šimůnek et al., 2008) was used to model the hydraulic behavior of the SF. HYDRUS-2D is a two-dimensional model for simulating the movement of water, heat, and multiple solutes in variably-saturated porous media. HYDRUS-2D numerically solves the Richards equation for multidimensional unsaturated flow:

$$\frac{\partial \theta}{\partial t} = \nabla[k \cdot \nabla(h - z)] - S \tag{1}$$

where t is time (T), z is the vertical coordinate (L), and S is a sink term ($L^3 L^{-3} T^{-1}$), defined as a volume of water removed from a unit volume of soil per unit of time due to plant water uptake. The unimodal van Genuchten–Mualem (VGM) model (van Genuchten, 1980) was used to describe the soil hydraulic properties of the two layers:

$$\Theta = \begin{cases} \frac{1}{(1+(\alpha|h|)^n)^m} & \text{if } h \leqslant 0 \\ 1 & \text{if } h > 0 \end{cases} \tag{2}$$

$$\Theta = \frac{\theta - \theta_r}{\theta_s - \theta_r}$$

$$K = \begin{cases} K_s \Theta^L [(1 - (1 - \Theta^{\frac{1}{m}}))^m]^2 & \text{if } h < 0 \\ K_s & \text{if } h > 0 \end{cases} \tag{3}$$

$$m = 1 - \frac{1}{n}$$

where Θ is the effective saturation ($-$), α is a shape parameter related to the inverse of the air-entry pressure head (L^{-1}), θ_s and θ_r are the saturated and residual water contents, respectively ($-$), n and m are pore-size distribution indices ($-$), K_s is the saturated hydraulic conductivity (LT^{-1}), and L is the tortuosity and pore-connectivity parameter ($-$).

While the soil hydraulic properties of the soil substrate were determined using the simplified evaporation method, those of the filter were optimized in the surrogate analysis framework. However, not all parameters were included in the optimization process. The residual water content θ_r was fixed to 0, considering that the filter is composed of coarse gravel, and the tortuosity L was set to 0.5, which is a common value in the literature. The initial range of the investigated parameters is reported in Table 1.

Feddes et al. (1978) defined S as:

$$S(h) = a(h) \cdot S_p \tag{4}$$

where $a(h)$ is a dimensionless water stress response function that depends on the soil pressure head h and has a range of values between 0 and 1, and S_p is the potential root water uptake rate. Feddes et al. (1978) proposed a water stress response function in which water uptake is assumed to be zero close to soil saturation (h_1) and for pressure heads larger (in absolute values) than the wilting point (h_5). Water uptake is assumed to be optimal between two specific pressure heads (h_2, h_3 or h_4), which depend on a particular plant. At high potential transpiration rates (5 mm/day in the model simulation) stomata start closing at lower pressure heads (h_3) (in absolute value) than at low potential transpiration rates (1 mm/d) (h_4). Parameters of the stress response function for a majority of agricultural crops can be found in various databases (e.g., Taylor and Ashcroft, 1972; Wesseling et al., 1991). Considering that the vegetation cover was mainly constituted of herbaceous plants, parameters reported for grass in Wesseling et al. (1991) were used in this study.

The local potential root water uptake S_p was calculated from the potential transpiration rate T_p. Beer's equation was first used to partition reference evapotranspiration, calculated using the Penman-Monteith equation (Allen et al., 1998), into potential transpiration and potential soil evaporation fluxes (e.g., Ritchie, 1972). The partitioning of evapotranspiration into potential transpiration and potential evaporation allows the computation of different actual fluxes in the soil-vegetation system. The Leaf Area Index (LAI) is needed to partition evaporation and transpiration fluxes. In this study, a LAI value of 2.29 as reported by Blanusa et al. (2013) for a *sedum* mix was used, considering its similarity with the installed vegetation. For a detailed explanation of evapotranspiration partitioning, please refer to Sutanto et al. (2012).

HYDRUS-2D allows for the consideration of a spatially variable root distribution. In this study, a homogeneous root zone within a depth of 15 cm was defined. The root density was assumed to be uniform inside the root zone and zero in the remaining part of the numerical domain. The total potential transpiration flux from a transport domain is equal in HYDRUS to potential transpiration T_p, multiplied by the surface length associated with vegetation.

This total potential transpiration flux is then distributed over the entire root zone for the computation of the actual root water uptake.

2.6. Numerical domain and boundary conditions

The two-dimensional domain had a length of 8.0 m and a depth of 0.75 m. The geotextile was not included in the model considering its negligible thickness, its limited hydraulic effect due to its high permeability, and that its sole function was to separate the soil substrate from the filter layer. The domain was discretized into two-dimensional triangular elements using the MESHGEN tool of HYDRUS-2D. The mesh was refined in the right part of the domain, where the effect of the surface runoff from the parking lot was simulated. This refinement was necessary in order to numerically accommodate the significant pressure head gradients generated by infiltration of runoff, and thus to reduce the mass balance errors. The generated FE mesh had 736 nodes and 1350 two-dimensional elements. The quality of the FE mesh was assessed by checking the mass balance error reported by HYDRUS-2D at the end of the simulation. Mass balance errors, which in this simulation were always below 1%, are generally considered acceptable at these low levels.

The surface of the SF was exposed to precipitation, evapotranspiration, and surface runoff from the impervious parking lot. As a result, in HYDRUS, two different boundary conditions were specified at the top of the modeled domain, as well as at its bottom (Fig. 3).

The "Atmospheric" boundary condition, which was assigned on the surface of the soil substrate (green line in Fig. 3), can exist in three different states: (a) precipitation and/or potential evaporation fluxes, (b) a zero pressure head (full saturation) during ponding when both infiltration and surface runoff occurs, and (c) an equilibrium between the soil surface pressure head and the atmospheric water vapor pressure head when atmospheric evaporative demand cannot be met by the substrate. The threshold pressure head, which was set to −10,000 cm, divides the evaporation process from the soil surface into two stages: (1) a constant rate stage when actual evaporation, equal to potential evaporation, is limited only by the supply of energy to the surface, and (2) the falling rate stage, when water movement to the evaporating sites near the surface is controlled by subsurface soil moisture and the soil hydraulic properties. In such conditions, actual evaporation, calculated as a result of the numerical solution of the Richards equation, is smaller than potential evaporation.

The "Variable Flux" boundary condition, which included both precipitation and measured surface runoff, was used in the area under the perforated pipe (red line in Fig. 3). Evaporation was excluded since most of the surface was covered by the perforated pipe, which reduced the exposure of the surface to wind and solar radiation.

A seepage face boundary condition (brown line in Fig. 3) was specified at the bottom left corner of the numerical domain to simulate the effect of the horizontal drain. A seepage face boundary acts as a zero pressure head boundary when the boundary node is saturated and as a no-flux boundary when it is unsaturated. A zero flux boundary condition (black line in Fig. 3) was applied to all remaining boundaries of the domain to simulate the effect of the impervious membrane placed at the bottom and on the sides of the SF.

The initial conditions were specified in terms of the soil water pressure head and were set to linearly increase with depth, from −90 cm at the top of the flow domain ($z = 0$) to −0.5 cm at the bottom ($z = -75$). The surface layers are assumed to be drier than the bottom layers since they are directly exposed to the atmosphere.

Table 1
Ranges of investigated parameters for the surrogate-based analysis.

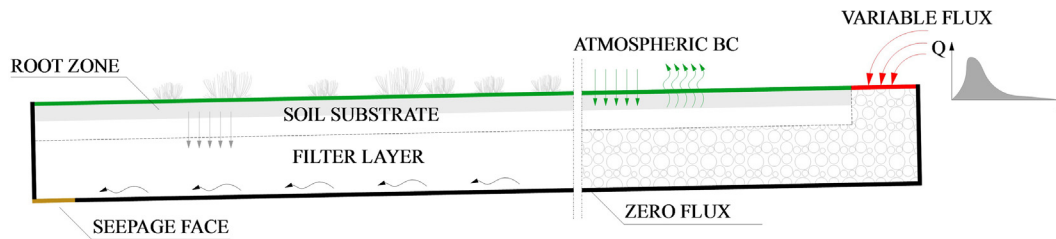| Parameter	Range
θ_s [$-$]	0.1–0.3
α [1/cm]	0.001–0.3
n_1 [$-$]	3.0–7.0
K_{s1} [cm/min]	30.0–100.0

Fig. 3. The spatial distribution of applied boundary conditions.

The numerical model is expected to be sensitive to the initial conditions only during the first few simulated days.

2.7. Surrogate based model

2.7.1. Kriging

There are two broad families of surrogate modeling techniques: Response Surface Surrogates (RSS) and Lower-Fidelity Surrogates (LFS). While RSS are data-driven techniques for approximating the response surface of high-fidelity (original) models based on a limited number of original model evaluations, LFS are essentially cheaper-to-run, alternative simulation models with different levels of accuracy (Razavi et al., 2012). As pointed out by Razavi et al. (2012) in their review paper, LFS outperforms RSS when the dimensionality of the problem is high and the response surface landscape is characterized by multimodality. In such circumstances, RSS would need a higher number of original model runs to correctly approximate the response surface. O'Hagan (2006) highlighted how the same number of design sites can lead to different parameters space coverages depending on the dimensionality of the problem. However, when the problem is low-dimensional and the response surface is characterized by a low or moderate multimodality, RSS are preferred since a limited number of high-fidelity model runs is required to build a reliable surrogate model.

The present study involves a SF model with four parameters to be investigated. Considering the low dimensionality of the problem, the kriging response surface approximation technique was used. Unlike other RSS, kriging models have their origins in mining and geostatistical applications involving spatially and temporally correlated data. The kriging technique has also been referred to in the literature as a Gaussian Process (GP) prediction (Rasmussen and Williams, 2006; Sacks et al., 1989). A Gaussian Process is formally defined as being a probability distribution over a (possibly infinite) number of variables, such that the distribution over any finite subset of them is a multi-variate Gaussian. As the Gaussian distribution is fully specified by its mean and covariance matrix, the GP is specified by a mean and a covariance function (Mackay, 1998). The mean is usually assumed to be zero, and, in such circumstances, the covariance function completely describes the GP behavior. One of the most attractive features of GP is that it treats the deterministic response of a computer model as the realization of a stochastic process, in particular a Gaussian random process, thereby providing a statistical basis for fitting. This capability provides a first approximation of uncertainty associated with each value predicted by the surrogate. Another advantage of kriging against other RSS techniques such as Artificial Neural Networks (ANN) or Support Vector Machines (SVM) is that kriging is an exact emulator. An exact emulator precisely predicts all design sites used to build the surrogate, while inexact emulators can introduce bias in such sites. As described by Razavi et al. (2012), an exact emulation is recommended for approximating the deterministic response of computer simulation models. Inexact emulators have smoothing capabilities that can help when the response surface is noisy (e.g., physical experiments), however this feature can lead to poor

approximation of the response surface when it is characterized by multiple local minima.

The kriging model is a combination of a polynomial model and a localized deviation model, which is based on a spatial correlation of samples (Eq. (4)):

$$y(x) = f(x) + Z(x) \tag{5}$$

where $y(x)$ is an unknown function of interest, $f(x)$ is an approximation function, and $Z(x)$ is the realization of a stochastic process with zero mean, the variance σ^2, and nonzero covariance. While $f(x)$ globally approximates the response surface through design sites, $Z(x)$ creates localized deviations. The covariance matrix of $Z(x)$ is given by Eq. (6):

$$Cov[Z(x^i), Z(x^j)] = \sigma^2 \Psi([R(x^i, x^j)]) \tag{6}$$

where Ψ is the $p \times p$ symmetric correlation matrix and $R(x^i, x^j)$ is the correlation function between two of the p sampled data points. $R(x^i, x^j)$ can assume different forms and is specified by the user. In this study, the Gaussian correlation function has been used (Eq. (7)):

$$R(x^i, x^j) = \exp\left(-\sum_{k=1}^{N} \tau_j |x_k^i - x_k^j|^2\right) \tag{7}$$

where N is the number of parameters, τ_j are the unknown correlation parameters used to fit the model, and x_k^i and x_k^j are the kth components of the sample points x^i and x^j. Correlation parameters τ_j are estimated using the maximum likelihood methodology. The "best" kriging model is found by solving a j-dimensional, unconstrained, nonlinear optimization problem. In this study, the PSO global optimization algorithm has been used to identify kriging parameters.

2.8. Design of experiments

The first step in the generation of a surrogate model is to sample the response surface at some specific design sites. This procedure is usually referred to in the literature as the Design of Experiments (DoEs). As pointed out by Razavi et al. (2012), a sufficiently large and well-distributed set of initial design sites is crucial for a successful application of a metamodeling framework. There are several DoEs methods available in the literature. Factorial design (Gutmann, 2001), Latin Hypercube Sampling (LHS) (McKay et al., 1979), and Symmetric Latin Hypercube Sampling (SLHS) (Ye et al., 2000) are the most commonly used. In this study, the LHS has been used. The size of the DoEs sample is strongly dependent on the complexity of the original response surface and computational budget available. The kriging model requires at least $N+1$ design sites to fit, while additional sites will improve the accuracy of the surrogate. Several relations were proposed in the literature to choose the size p of the initial sample (e.g., Gutmann, 2001; Regis and Shoemaker, 2004). In this study, the relation proposed by Jones et al. (1998) has been used (Eq. (8)):

$$p = 10N \tag{8}$$

Considering that the number of investigated parameters was 4, 40 sampling points were generated using the LHS.

2.9. Approximation uncertainty framework

The surrogate model fitted on a DoEs sample is only the first approximation of the original response function. Its accuracy can be improved using further original model runs (*infill points*) in addition to the initial sampling plan. The distribution of *infill points* strongly depends on the complexity of the original response surface and on the type of analysis conducted. When the purposes of the analysis of the surrogate model includes uncertainty and sensitivity analyses, it is necessary to have an accurate global approximation of the response surface. The adaptive-recursive framework relies on the assumption that the optimal solution of the surrogate represents well the original model. However, this is not always true, especially when the response surface is characterized by high multimodality. When the approximation of the response surface by the surrogate model is limited, this framework is not recommended for the uncertainty and/or sensitivity analysis. Jones (2001) concluded that the adaptive-framework is helpful at best for local optimization.

In this study, the approximation uncertainty framework was applied to address the shortcoming of the adaptive-recursive framework, which considers uncertainties associated with the approximation. RSS, such as kriging, explicitly provide a measure of uncertainty since they treat the deterministic response of a computer simulation as the realization of a stochastic process. The model can then be evaluated at points with the highest uncertainty, which can then be included among the design sites. Although globally convergent, such an approach requires an impractically large number of original function evaluations. An effective uncertainty based framework should balance exploitation (i.e., fine tuning of a good solution) and exploration (i.e., reducing the overall uncertainty of the surrogate). The expected-improvement approach (Schonlau, 1997) was used in this study. An expected-improvement is a measure that statistically quantifies the obtained improvement when a given point is evaluated by the original model and added to design sites. For a complete description of the expected-improvement approach please refer to Schonlau (1997).

In this study, the expected-improvement approach was used to add 15 *infill points* to the initial design sites. In order to have good accuracy, the surrogate was refitted after each new original model evaluation (Razavi et al., 2012).

2.10. Surrogate validation

Validation of the RSS model is important for evaluating the reliability of the surrogate. Although exact emulators such as kriging exactly interpolate the response surface at design sites, their accuracy in unexplored regions of the parameter space must be evaluated. The validation can be conducted by evaluating the agreement between values of the variable of interest predicted by both the surrogate and original models on an independent set of sample points. Cross validation strategies such as *k*-fold and leave-one-out cross validation have also been used in the literature (Wang and Shan, 2007). In the present study, an independent set of sample points was generated using the LHS and used to validate the model. Ten points were used to carry out the validation process. The Pearson coefficient R^2 was used to assess the agreement between predicted and modeled values. As suggested by Forrester et al. (2008), a value of the correlation coefficient higher than 0.8 indicates a surrogate model with good predictive capabilities.

2.11. Global Sensitivity Analysis (GSA)

A sensitivity analysis (SA) can identify the most influential parameters, their interactions, and how these parameters affect the output (Saltelli et al., 2005). Most SAs performed in the literature of environmental sciences are the so-called 'one-at-a-time' (OAT) sensitivity analyses, performed by changing the value of parameters one-at-a-time while keeping the other parameters constant (Cheviron and Coquet, 2009; Houska et al., 2013; Rezaei et al., 2015). However, when the model includes interactions between multiple parameters, results of the OAT analysis are inaccurate because parameter interactions can be globally identified only by simultaneously changing multiple parameters. For this reason, when the property of a model is *a priori* unknown, a Global Sensitivity Analysis (GSA) is always preferred (Saltelli and Annoni, 2010). Practitioners call this analysis a model-free setting, which means that a particular application does not depend on particular assumptions regarding the behavior of the model, such as linearity, monotonicity, etc (Saltelli and Annoni, 2010).

Variance-based methods aim to quantify the amount of variance that each parameter contributes to the unconditional variance of the model output. In Sobol's method, these measures are represented by Sobol's sensitivity indices (SIs). These indices give quantitative information about the variance associated with a single parameter or with interactions of multiple parameters. For a more complete explanation about Sobol's method, please refer to Sobol' (2001). Sobol's sensitivity indices are expressed as follows:

$$FirstOrder\ S_i = \frac{V_i}{V} \tag{9}$$

$$SecondOrder\ S_{ij} = \frac{V_{ij}}{V} \tag{10}$$

$$Total\ S_T = S_i + \sum_{j \neq i} S_{ij} + \dots \tag{11}$$

where V_i is the variance associated with the *i*th parameter and V is the total variance. The first-order index, S_i, is denoted in the literature as the "main effect." When the model is additive, i.e., when it does not include interactions between input factors, the first-order index is sufficient for decomposing the model's variance. For additive models, the following relation is valid:

$$\sum_i S_i = 1 \tag{12}$$

On the other hand, the total effect index, S_T, gives information about a non-additive part of the model. $S_{Ti} = 0$ is a condition necessary and sufficient for X_i to be non-influential. For an accurate description of the calculation of Sobol's indices please refer to Saltelli et al. (2010).

When the model is nonlinear, as most environmental models are, Sobol's indices are calculated using Monte Carlo integrals. Obviously, the accuracy in the estimation of integrals becomes more accurate as the number of samples increases, which also increases the computational cost of the SA. However, this limitation is avoided when using a surrogate model since the computational cost associated with the evaluation of a large number of samples is very low (O'Hagan, 2006; Oakley and O'Hagan, 2004). For this reason, 1000 samples for a total of 30,000 surrogate model runs were used in this study. To sample the parameters' space we used Sobol's quasi-random sampling technique (Sobol', 2001).

In order to assess the accuracy of the estimations of the sensitivity indices, the bootstrap confidence intervals (BCIs) (Efron and Tibshirani, 1986) were estimated. The basic idea of the bootstrapping is that the sample contains all available information about the underlying distribution. In our particular case, we were interested in computing the uncertainty of estimated sensitivity indices. However, since their distribution is unknown it is not possible to compute the confidence intervals analytically. The rationale of the bootstrap method is to replace the unknown distribution with

its empirical distribution and to compute the sensitivity indices using a Monte Carlo simulation approach where samples are generated by resampling the original sample used for the sensitivity analysis. In our case, the samples used for the GSA were sampled 1000 times with replacement, whereby Sobol's indices were calculated for each resampling. In this way, 95% confidence intervals are constructed using the percentile method and the moment method (Archer et al., 1997).

2.12. Particle Swarm Optimization

Numerous applications of inverse modeling for the estimation of soil hydraulic properties exist in the literature (Abbaspour et al., 2004; Hopmans et al., 2002; Vrugt et al., 2008; Vrugt et al., 2004). The gradient methods (Marquardt, 1963) have been most widely used among hydrologists and soil scientists. However, these methods are sensitive to the initial values of optimized parameters and the algorithm often remains trapped in local minima, especially when the response surface exhibits a multimodal behavior. These considerations inspired researchers to develop and use global optimization techniques such as the annealing-simplex method (Pan and Wu, 1998), genetic algorithms (Ines and Droogers, 2002), shuffled complex methods (Vrugt et al., 2003), and ant-colony optimization (Abbaspour et al., 2001), among many others.

In this paper, a global search method based on Particle Swarm Optimization (PSO) (Kennedy and Eberhart, 1995) was used. This method simulates the behavior of a flock of birds collectively foraging for food (i.e., searching for the optimum of the objective function). In their recent study, Brunetti et al. (2016b) used PSO to estimate the soil hydraulic properties of a permeable pavement with satisfactory results. PSO is a relatively new algorithm for evolutionary computation methodology, but its performance has proven to be comparable to various other more established methodologies (Kennedy and Spears, 1998; Shi et al., 1999). One of the main advantages of PSO is the easiness of its implementation (Liang et al., 2006). A detailed description of the PSO algorithm is given in Shi and Eberhart (1998).

In PSO, each particle represents a possible solution of the problem. First, particles are placed in the search space, each characterized by a particular value of the objective function. Each particle then changes its position after exchanging information about its own current and best positions with other members of the swarm. The next iteration starts after all particles have changed their positions. The most important parameters in the PSO are c_1, c_2, and w. c_1 and c_2 are constant parameters known as the cognitive and social parameters, respectively, which drive the search behavior of the algorithm. Depending on the values of c_1 and c_2 the PSO can be more or less "responsive". However, their values should be selected carefully because large values of these parameters can lead to instabilities in the algorithm. w is the inertia-weight, which plays a key role in the optimization process by providing balance between exploration and exploitation. In PSO, each particle is influenced by its nearest neighbors. The arrangement of neighbors that influence a particle is called the *topology* of the swarm. Different types of neighborhoods are reported in the literature (Akat and Gazi, 2008). In this study, the *all* topology is used, in which the neighborhood encompasses the entire swarm. The PSO parameters used in this study for both scenarios are reported in Table 2 and are as suggested by Pedersen (2010).

Table 2
Parameters used in the PSO optimization.

Swarm size	c_1	c_2	w
63	−0.73	2.02	−0.36

2.13. Objective function

The Nash-Sutcliffe efficiency (NSE) index (Nash and Sutcliffe, 1970) was used to evaluate the agreement between measured and modeled hydrographs and as the variable of interest in the surrogate analysis:

$$NSE = 1 - \left[\frac{\sum_{i=1}^{T} (Q_i^{obs} - Q_i^{mod})^2}{\sum_{i=1}^{T} (Q_i^{obs} - Q_{mean}^{obs})^2} \right] \tag{13}$$

where Q_i^{obs} is the ith measured value, Q_i^{mod} is the ith simulated value, and Q_{mean}^{obs} is the mean value of observed data. The *NSE* index ranges between $-\infty$ and 1.0, is equal to 1 in case of perfect agreement, and generally, values between 0.0 and 1.0 are considered acceptable (Moriasi et al., 2007). The *NSE* index was used because it is often reported to be a valid measure for evaluating the overall fit of a hydrograph (Sevat et al., 1991).

It is important to emphasize that subsurface outflow from a LID system is among the most important outputs in the analysis of urban drainage systems. In our case, the stormwater filter was impervious at the bottom and hydraulically connected with the sewer system. An accurate numerical reconstruction of the subsurface hydrograph is thus fundamental in order to quantify its effect on the drainage system.

3. Results and discussion

3.1. Evaporation method

Soil hydraulic properties measured using the evaporation method are displayed in Fig. 4. The retention data point close to log (|h|) = 4 (h in cm) was obtained by using the air-entry pressure head of the ceramic cup of the tensiometers. Measured retention points were not available in the very dry range, between 2.7 and 3.8, since cavitation occurred in the tensiometers. The behavior of the retention curve appears to be sigmoidal and characterized by a clearly identifiable air-entry pressure head at log (|h|) = 2 (h in cm). Below this pressure head, the soil quickly desaturated, indicating a narrow pore-size distribution. Measured points of the hydraulic conductivity function were sparser and concentrated in the dry range between volumetric water contents of 0.10 and 0.20. The measured soil porosity and bulk density were 0.44 and 1.59 g/cm³, respectively.

The unimodal van Genuchten-Mualem model (van Genuchten, 1980) was fitted to measured points using the HYPROP-FIT software. The *RMSE* values for retention and conductivity functions were 0.04 (cm³cm⁻³) and 0.6 (in log K, cm/day), respectively. The VGM function (full lines in Fig. 4) described the retention data well, especially in the dry and medium-wet regions (volumetric water contents of 0.5–0.3), while it introduced some bias near saturation where it poorly described the sharp increase in water retention at the air-entry pressure head. However, the low *RMSE* value was considered acceptable for the purposes of the present study. The *RMSE* value for the hydraulic conductivity was higher, indicating a slightly worse performance of the VGM function in describing the hydraulic conductivity of the substrate. The estimated soil hydraulic parameters (reported with their confidence intervals in Table 3) were used in HYDRUS-2D to model the hydraulic behavior of the soil substrate.

3.2. Kriging approximation of the response surface

The DoEs sample, generated with the LHS technique, was used to build the first approximation of the response surface for the investigated soil hydraulic parameters. First, the HYDRUS-2D
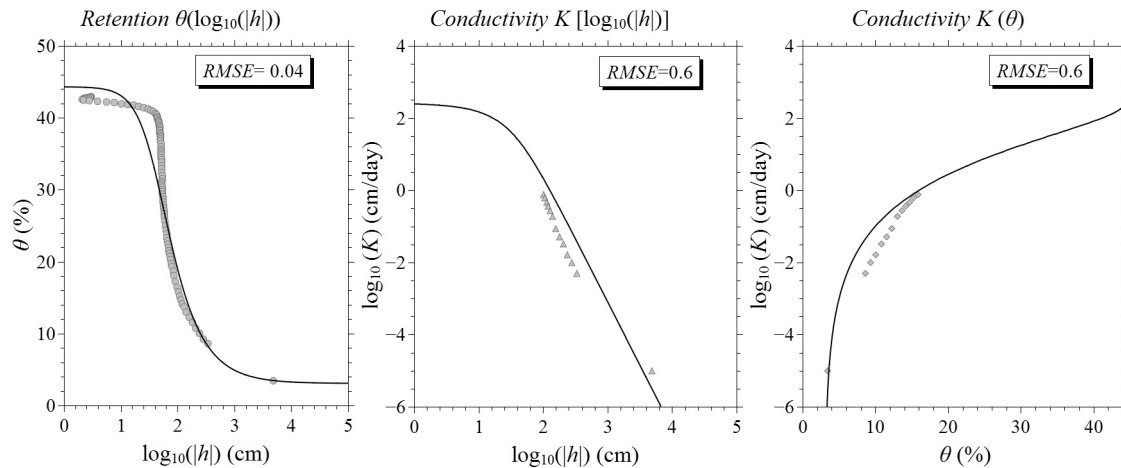
Fig. 4. Measured values and modeled functions of soil water retention, θ ($\log_{10}(|h|)$) (left) and the unsaturated hydraulic conductivity, $K(\log_{10}(|h|))$ (center) and $K(\theta)$ (right). Symbols represent the measured values, and full lines the fitted VGM functions.

Table 3
Estimated soil hydraulic parameters and their confidence intervals for the bimodal hydraulic function.

Parameter	2.5%	Estimated value	97.5%
θ_r (−)	0.02	0.03	0.04
θ_s (−)	0.43	0.44	0.45
α (1/cm)	0.021	0.025	0.029
n (−)	1.84	1.97	2.10
K_s (cm/day)	200	260	320
L (−)	−0.63	−0.44	−0.25

model was executed 40 times (Eq. (8)), and the *NSE* index was computed for each run and stored in a 1D array. A single run of the original HYDRUS-2D model required almost 1 min of CPU time on a laptop equipped with a CPU Intel® Core i7-4700 MQ 2.40 GHz processor and 8 GB of RAM. Next, the LHS sample and the *NSE* array were used in the PSO optimization framework to estimate the kriging parameters. To check its accuracy, the obtained kriging model was validated on another independent sample generated with the LHS. As shown in Fig. 5, the validation sample covered values of *NSE* ranging from 0.2 to 0.8, providing information about the response surface for both less and more accurate portions of the parameters space.

At the first inspection, the kriging model based on the initial sample exhibited a moderate accuracy. The determination coefficient R^2 for the initial kriging model was 0.91, which already indicated an overall accuracy of the surrogate model (Forrester et al., 2008). This confirmed the good coverage of the DoEs sample. However, as shown in Fig. 5, the surrogate, while being highly accurate for low values of the objective function, introduced a significant bias for high values of *NSE*, which are those of interest in an optimization framework. The regression line for the initial surrogate (a dashed grey line in Fig. 5) almost overlapped the bisector (a black line in Fig. 5), which indicates a perfect agreement between the surrogate and the original model in the range of 0.2–0.4, while it underestimated values of the response surface in the region around 0.8. The underestimation of the response surface values in the region where optimal parameter values are likely located could influence the next surrogate-based optimization of soil hydraulic properties.

To increase the accuracy of the kriging model, the approximation uncertainty framework was used next. As described in the methodology section, 15 *infilled* points were added to the initial design sites using the expected improvement approach. As shown in Fig. 5 and as expected, the infilled kriging model outperformed
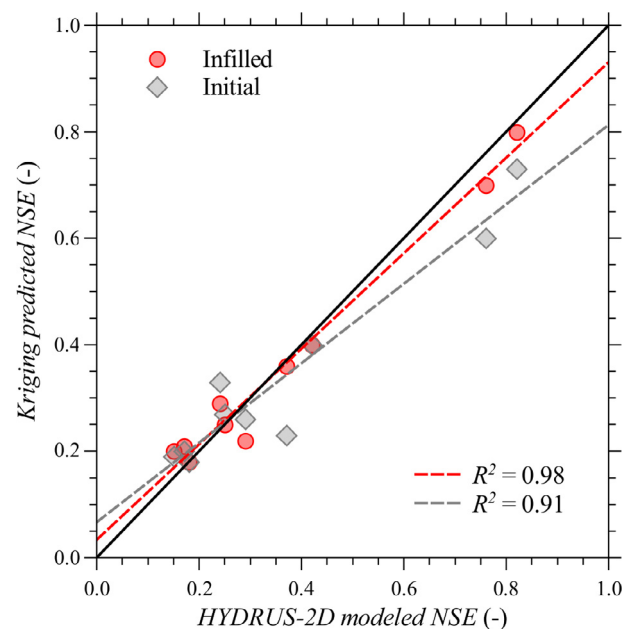
Fig. 5. Comparison between the HYDRUS-2D and kriging-predicted values of the *NSE* for the validation sample. The initial (grey diamonds) and infilled (red circles) kriging models are compared. A bisector (a black line) and regression lines for the initial (a dashed grey line) and infilled (a dashed red line) kriging models are reported.

the initial kriging model. The determination coefficient R^2 increased to 0.98, indicating that the infilled kriging improved the description of the response surface. This behavior was confirmed by the regression line (a dashed red line in Fig. 5), which almost overlapped a bisector line. Moreover, the accuracy of the kriging model improved for high values of *NSE*, which are those of interest in an optimization process, while remaining similarly high for low values of *NSE*. This global accuracy of the surrogate is fundamental for the GSA, which explores the response surface landscape. However, it should be noted that even when the surrogate accuracy improves after applying the approximation uncertainty framework, a certain degree of bias remains. A possible solution to further investigate this bias would be to increase the validation sample size. However, there are no clear indications in the literature regarding the size of the validation sample in similar problems (i.e. optimization and sensitivity analysis of soil hydraulic properties), making the choice rather subjective. Moreover,

increasing the validation sample size would significantly increase the computational cost of the analysis. In our particular case, in view of all the possible sources of uncertainty that affect the analysis, the validation of the surrogate-based optimized parameters against an independent set of data, performed towards to end of the study, was specifically intended to provide a final check on the accuracy of the estimated parameters. Considering the relatively high accuracy of the surrogate, no additional points were thus added to the design sites considering the relatively high accuracy of the surrogate, and the final surrogate was used for the GSA and optimization.

3.3. Global Sensitivity Analysis

The validated kriging model was next used in the GSA. Sobol's sensitivity indices, with their confidence intervals for each parameter, are reported in Table 4.

The sensitivity analysis revealed that the model was additive. This was confirmed by the sum of the first-order indices, which was almost 1, and by negligible differences between the first-order and total-effect indices for each parameter. An additive model $Y = f(X_1, X_2, \ldots, X_N)$ can be decomposed into a sum of N functions, where N is the number of parameters. This means that the effects of interactions between model parameters on model results were negligible.

As shown in Table 4, the most influential parameter was the shape parameter α. Its first-order (S_1) and total effect (S_T) indices were more than an order of magnitude higher than corresponding indices for the second most influential parameter K_s. The pore-size distribution index n and the saturated water content θ_s exhibited the lowest sensitivity, indicating their marginal role on the output's variance. Moreover, since their total effects were almost zero, these parameters can be fixed to any feasible value in the parameter space without affecting the value of the objective function, reducing the dimensionality of the inverse problem to only two parameters, α and K_s. Such results are very useful in an optimization framework, since they can simplify the parameter estimation procedure. Some of the total effect indices were only slightly larger than the first order indices. This is mainly due to approximation in the numerical integration of the total unconditional variance (Sobol', 2001).

It must be emphasized that additivity is quite unusual for environmental models, which are generally characterized by high nonlinearity and interactions between parameters (Brunetti et al., 2016b; Nossent et al., 2011). In our particular case, the dominant effect of the α parameter on the hydrograph makes it difficult to identify interactions between parameters. This may also indicate that water flow in the filter layer deviates from the traditional Darcian behavior and involves other physical processes, such as preferential and film flows. In such circumstances, some parameters can exhibit a negligible effect on the model's response. This may indicate that the proposed modeling approach could be affected by *model discrepancy*, a concept introduced by Kennedy and O'Hagan (2001) to assess sources of uncertainty due to underlying missing physics, numerical approximations, and other inaccuracies

of the model. When the *model discrepancy* is not directly accounted for, the model parameters can be treated as simple tuning parameters, which often act as a simplified surrogate for some more complex process that is not modeled in the simulator (Brynjarsdottir and O'Hagan, 2014). In our case, it is plausible that the shape parameter α acted as a tuning parameter, condensing and representing more complex phenomena, namely preferential and film flows. It must be emphasized that the surrogate-based sensitivity analysis can be extremely useful in detecting different sources of uncertainties. Future researches should explicitly account for *model discrepancy* in the analysis (Brynjarsdottir and O'Hagan, 2014) to examine its impact on the model's behavior, or perform the same type of analysis using more complex models which account for preferential flows in the filter layer.

As mentioned in the methodology section, the GSA required 30,000 evaluations of the surrogate model. The computational cost of the kriging-based sensitivity analysis was limited to 1–2 s on a laptop equipped with a CPU Intel® Core i7-4700 MQ 2.40 GHz processor and 8 GB of RAM. On the other hand, since a single HYDRUS-2D model run required approximately 1 min, the same type of GSA performed using the original HYDRUS-2D model would have required approximately 21 days of continuous computation. This clearly represents one of the main advantages of surrogate-based modeling: performing the same type of analysis with negligible computation time and a similarly good level of accuracy.

3.4. Kriging-Based optimization

Using the results of the GSA, only shape parameter α and the saturated hydraulic conductivity K_s were optimized. The saturated water content θ_s and the pore-size distribution index n were assumed to be 0.15 and 3.2, respectively, considering that the filter layer consisted of coarse gravel, usually characterized by reduced porosity and narrow pore-size distribution. The soil hydraulic parameters of the filter layer, including the optimized parameters, are summarized in Table 5. The filter layer exhibited both a high value of the saturated hydraulic conductivity K_s (90 cm/min) and a very low value of the shape parameter α (0.001 1/cm).

The estimated parameters indicated that the hydraulic behavior of the filter layer was characterized by high flow rates and negligible retention capacity, which are both typical for coarse textured media. The optimized parameter values are similar to those reported in Brunetti et al. (2016b) for the base layer of a permeable pavement. In that study, the base layer consisted of crushed stones and was modeled using either the classical VGM function or the dual-porosity approach to account for preferential flow. Specifically, for the unimodal VGM function, the authors reported a value of 0.023 1/cm for the shape parameter α and a saturated hydraulic conductivity K_s of 68.7 cm/min. Moreover, the plausible occurrence of film flow in the filter layer, which can support very high flow rates, especially at near-zero matrix potential (Tokunaga, 2009), needs to be contemplated. Under such circumstances, the hydraulic behavior of the material tends to deviate from the typical Richard's type flow, and the optimized parameters attempt to approximate a combination of fingering and film flow that likely occur in this layer.

Fig. 6 shows a comparison between the measured and modeled hydrographs for the optimization period. The PSO resulted in the *NSE* value of 0.85, which confirmed the accuracy of the measured and estimated parameters. As reported by Moriasi et al. (2007), values of *NSE* between 0.75 and 1.0 indicate a very good agreement between hydrographs, and an adequate model calibration. The model was able to correctly reproduce the fast hydraulic response of the hydrograph during precipitations and to reasonably estimate peak flows. The insert of Fig. 6 shows the simulated against measured SF outflows. The same plot also shows a bisector line, which

Table 4
The first-order (S_1) and total (S_T) effect indices (in a decreasing order) with their bootstrap confidence intervals (BCI) for the soil hydraulic parameters.

Parameter	S_1	S_1 (BCI)	S_T	S_T (BCI)
α [1/cm]	0.93	0.24	0.94	0.05
K_s [cm/min]	0.04	0.08	0.05	0.007
n [−]	0.01	0.02	0.008	0.001
θ_s [−]	0.002	0.01	0.001	0.001
Sum	≈1.0		≈1.0	

Table 5
Unimodal VGM parameters for the filter layer. The shape parameter α and the saturated hydraulic conductivity K_s were estimated using the PSO algorithm.

Soil hydraulic parameters						
Layer	θ_r (−)	θ_s (−)	α (1/cm)	n (−)	K_s (cm/min)	L (−)
Filter	0	0.15	0.001	3.2	90	0.5
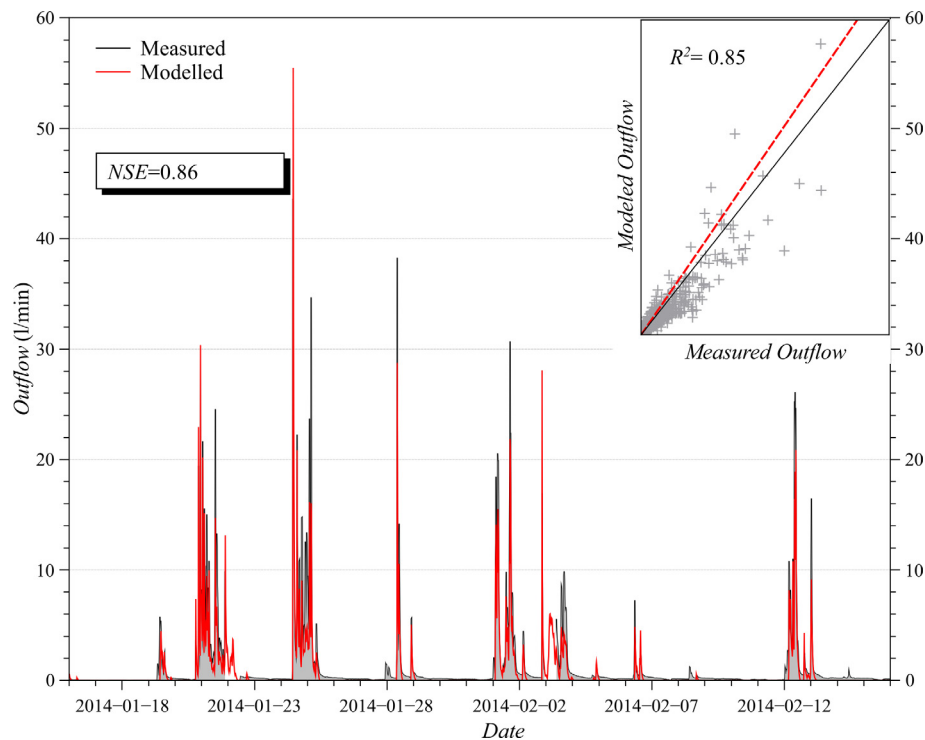
Fig. 6. A comparison between measured and simulated outflows versus time and against each other (in the insert) for the calibration period. The full and dashed lines in the insert are a bisector and linear regression line, respectively.

indicates a perfect agreement between simulated and measured outflows, and a linear regression line. The good performance of the model is confirmed by the determination coefficient $R^2 = 0.85$. The comparison between the bisector and regression lines indicates that, in general, the model slightly overestimated the outflow.

A careful inspection of simulated fluxes revealed that the model tends to underestimate low flows (Fig. 6). This behavior could be related to the coarse nature of the filter layer, which closely resembles "fractured aquifers". Typical breakthrough curves for fractured aquifers are characterized by early breakthrough and long tailing (Geiger et al., 2010). This is due to a delayed response in the matrix to pressure head changes that occur in the surrounding fractures. Brattebo and Booth (2003), Brunetti et al. (2016b), and Fassman et al. (2010) observed a similar behavior in permeable pavements, the base and sub-base layers of which are composed of crushed stones. In such circumstances, more complex models are needed to simultaneously describe fast preferential flow and the matrix-fracture interactions in the filter layer (Brunetti et al., 2016b).

Since the computational time associated with a single surrogate model evaluation was negligible, the approximate response surface was investigated. Fig. 7 shows the α-K_s response surface obtained using a regular grid of 40,000 points. The darkest areas represent regions of the parameter space with high values of NSE. At the first inspection, the response surface was characterized by a moderate multimodality. As shown in Fig. 7, optimal solutions were concentrated in the left part of the plot for values of α between 0.001 and 0.05. For α values > 0.05, the objective function dropped quickly to
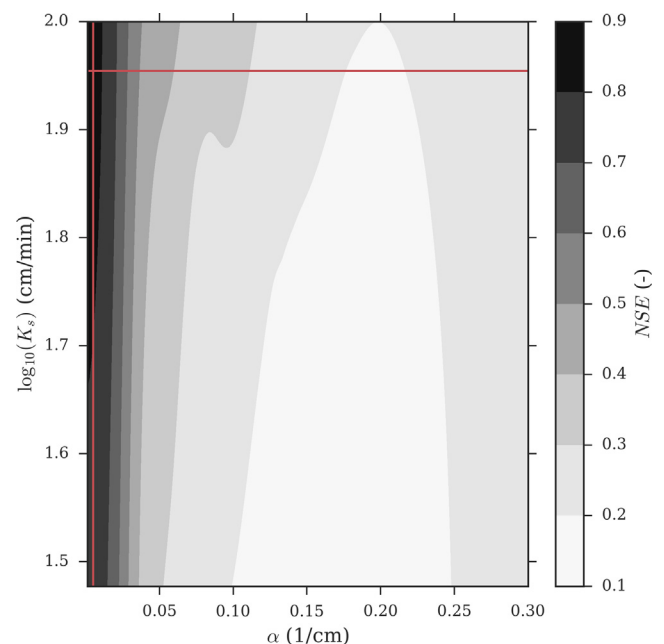
Fig. 7. The α-K_s response surface obtained using a regular grid of 40,000 points. The red lines indicate the cross sections reported in Fig. 8.

0.3–0.4. The *NSE* values slowly increased for values of α > 0.2. This can be expected since the α parameter for gravels usually has relatively high values. However, in our case, high values of α were not able to accurately reproduce the hydraulic behavior of the SF. For large α values, the filter layer quickly desaturates and increases its retention capacity. This effect delays the hydraulic response of the system to precipitation events. On the contrary, the use of low α values delays the desaturation of the filter layer, thus reducing its retention capacity (Cey et al., 2006). This makes the filter layer more responsive to precipitation events, which was the behavior observed in the measured hydrograph. On the other hand, the response surface exhibited limited variability in the K_s direction, since high values of *NSE* were guaranteed for a broad range of saturated hydraulic conductivity values.

These results confirmed the findings of the GSA, which clearly indicated that the variance of the objective function was mainly driven by the shape parameter α, with only a limited influence of K_s. This behavior is shown in detail in Fig. 8.

Fig. 8 shows horizontal (K_s = 90 cm/min) and vertical (α = 0.001 1/cm) cross-sections (red lines in Fig. 7) through the response surface. Yellow rectangular areas are expanded in the right part of the plot. With respect to K_s, the optimum was not clearly identifiable at the first inspection. The values of the objective function ranged between 0.8 and 0.85 in the entire range of the saturated hydraulic conductivity, indicating its limited effect on the response surface. The area around the PSO-optimized value of K_s (90 cm/min) is expanded in the bottom-right corner of Fig. 8. From this plot, it is evident how the PSO algorithm well identified the optimal value K_s, even for a flat profile.

Conversely, Fig. 8 shows a completely different behavior for the α-*NSE* profile, for which an optimal region was identified in the left part of the plot for low values of the α parameter. While the gradient of the curve seemed to approach a maximum, it was not possible to clearly identify the optimum, which may have been outside of the range imposed on the α parameter. As previously discussed, this behavior could be related to a deviation from the Darcian flow in the filter layer, which requires a more complex modeling

approach. The further analyzes of the response surface indicated that values of α over 0.01 1/cm corresponded to a marked decrease of *NSE*. This is evident from the expanded area in the top-right corner of Fig. 8. This finding is in agreement with the results of the GSA, which identified α as the most influential parameter.

In order to verify whether additional soil hydraulic parameters, such as the saturated water content θ_s and the pore-size distribution index *n*, influenced the optimum, a surrogate-based optimization, which considered four soil hydraulic parameters was carried out. The results of the optimization are listed in Table 6.

As shown in Table 6, the newly estimated parameters are very similar to those estimated when θ_s and *n* were fixed. The saturated water content was 0.17, which is slightly higher than the previously fixed value. Conversely, the pore-size distribution index *n* was slightly lower, but the difference was again very small. The two most sensitive parameters α and K_s had some small changes, however overall results are in a good agreement with those reported previously. Again, the filter layer exhibited a relatively high permeability and a low value of the α parameter, which is no longer situated at the border of the evaluated parameter space. Since α is related to the inverse of the air-entry pressure head, this suggests that its value is finite and could potentially be measured. These numerical differences could be related to the effects of interactions between parameters, which, even if small in magnitude as demonstrated by the GSA, can affect the parameters estimation. Including these parameters in the optimization process can potentially reduce the parameters uncertainty and help in better defining the problem.

3.5. Model validation

In order to evaluate the reliability of the estimated parameters, the model was validated using another independent set of experimental data. Fig. 9 shows a comparison between measured and modeled hydrographs during the validation period.

The value of the objective function was *NSE* = 0.8, which again confirmed the adequacy of the estimated parameters. The descrip-
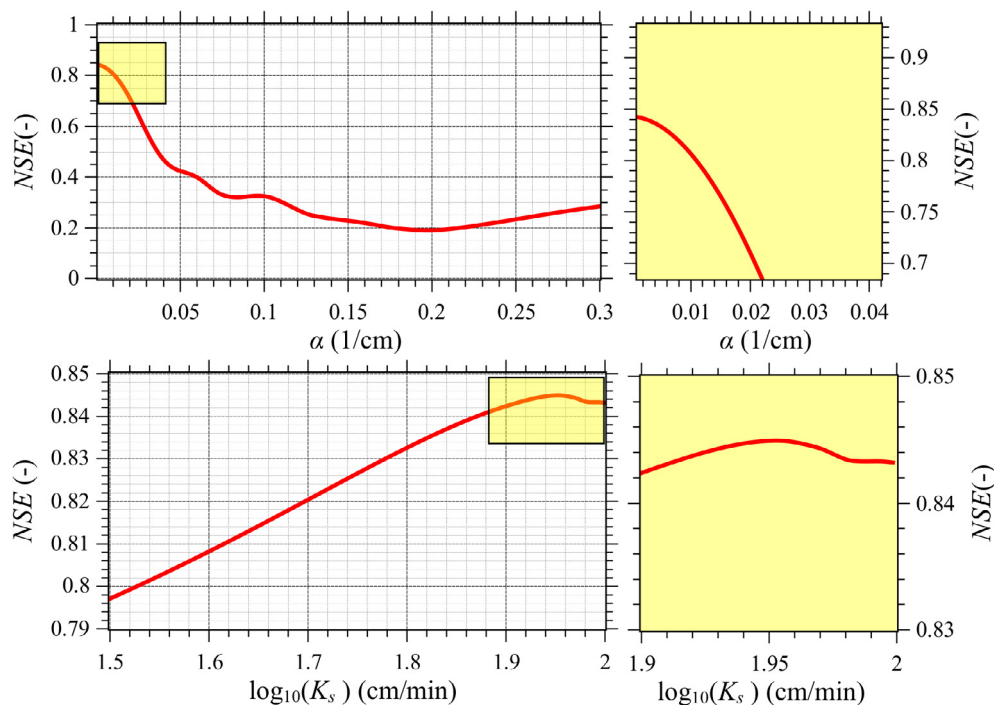

Fig. 8. Horizontal [K_s = 90 cm/min] (top), and vertical [α = 0.001 1/cm] (bottom) response surface cross-sections. The yellow rectangular areas for both plots are expanded on the right.

Table 6

Unimodal VGM parameters for the filter layer. The saturated water content θ_s, the shape parameters α and n, and the saturated hydraulic conductivity K_s were estimated using the PSO algorithm.

Soil hydraulic parameters					
Layer	θ_r (−)	θ_s (-)	α(1/cm)	n (−)	K_s (cm/min)	l (−)
Filter	0	0.17	0.003	3.1	89	0.5
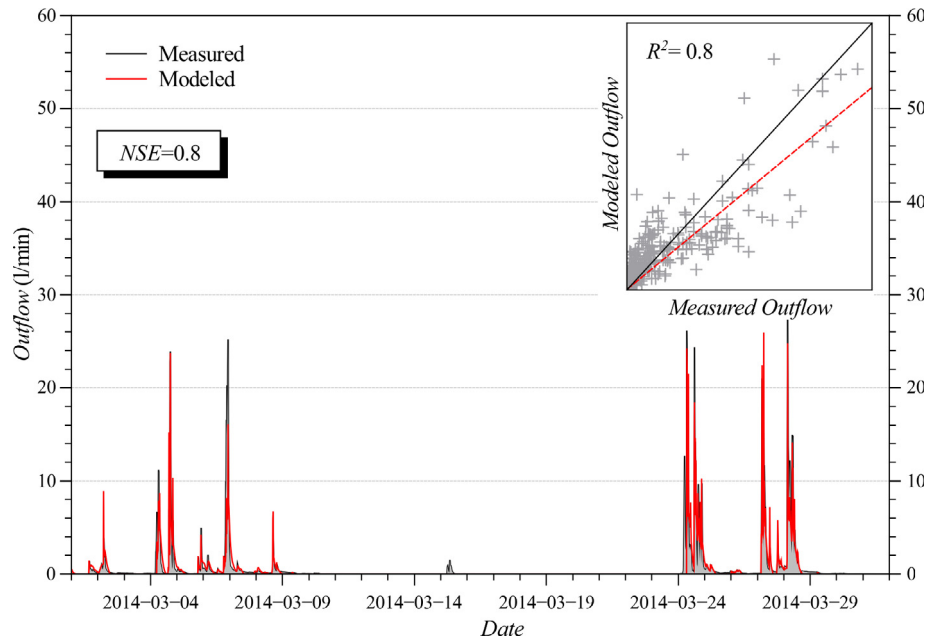
Fig. 9. A comparison between measured and simulated outflows versus time and against each other (in the insert) during the validation period. The full and dashed lines in the insert are a bisector and linear regression line, respectively.

tion of the hydraulic behavior of the stormwater filter during rainfall events was satisfactory. This capability of the calibrated model to correctly describe the hydraulic behavior of the system is important when dealing with the analysis of combined traditional drainage systems and LID techniques. A correct description of the hydrograph during precipitation events gives information about the lag time and the intensity of peak flow, which are fundamental for both a comprehensive hydraulic analysis of drainage systems, and for the evaluation of benefits of LIDs implementations. The model was not able to reproduce outflow induced by the precipitation event on March 15. This may be related to an overestimation of actual evapotranspiration calculated using values from the literature for albedo, LAI, and a hypothetical roots distribution, which could result in an overestimation of the storage capacity of the SF at the beginning of the precipitation event, which had a total volume of 6 mm. As a result, the model predicted that the SF retained all the precipitation volume. A better characterization of evapotranspiration could help in increasing the accuracy of the model, which was already high. As for the optimization data set, the model poorly described the long tailing behavior of the hydrograph after precipitations. This behavior is particularly evident for the precipitation event on March 28.

4. Conclusions and summary

The aim of this study was to demonstrate the benefit of surrogate-based modeling in the numerical analysis of Low Impact Development techniques. In particular, the unsaturated hydraulic properties of a contained stormwater filter installed at the University of Calabria were evaluated in the study. The kriging technique was used to approximate the deterministic response of the widely

used mechanistic model HYDRUS-2D, which was used to simulate the variably-saturated hydraulic behavior of the filter. In order to reduce the dimensionality of the inverse problem, the simplified evaporation method was used to determine the unsaturated soil hydraulic properties of the soil substrate placed on the top of the filter layer. The Nash-Sutcliffe efficiency index was used both to compare the simulated and measured outflows, and as the variable of interest for the construction of the response surface.

The PSO heuristic algorithm was used to estimate the kriging parameters based on an initial set of design sites obtained using Latin Hypercube Sampling. The approximation uncertainty framework improved the accuracy of the surrogate model by using the expected-improvement approach to select additional points to the initial design sites. The kriging model was validated against an unexplored set of points with satisfactory results. The obtained surrogate was then used to perform a Global Sensitivity Analysis of the hydraulic parameters of the filter layer based on Sobol's method, with a negligible computational cost. The sensitivity analysis revealed that the model is additive, and that two soil hydraulic parameters, the shape parameter α and the saturated hydraulic conductivity K_s, mainly affect the hydraulic response of the filter layer. These two parameters were estimated using the PSO algorithm with a NSE value of 0.85, which indicated an good accuracy of the model. Moreover, the analysis of the response surface confirmed the results of the GSA, identifying α as the most influential parameter. The reliability of the surrogate-based analysis was evaluated by validating the optimized parameters on an independent dataset of measured outflows. A NSE value of 0.8 confirmed the reliability of the HYDRUS-2D model calibrated using the kriging technique. In both the optimization and validation, the model poorly described the long-tailed behavior of the hydrograph after precipitations. This could be related to the model inadequacy in

describing both the film and preferential flows, and the matrix-fracture interactions that occurs in the filter layer. This suggests that more complex models are needed to better describe the hydraulic processes involved.

One of the most widespread criticism against the use of mechanistic models is their computational cost, which limits their adoption. This study has demonstrated how a surrogate-based analysis can provide an effective solution in overcoming this limitation. In this paper, the kriging technique was used for highly expensive computational analyses, such as the GSA and the PSO, with good results. The sufficiently accurate reproduction of measured hydrographs, which is extremely important in the analysis of LIDs, confirmed the benefit and reliability of surrogate-based analysis.

This novel study represents the first contribution towards the use of surrogates for LIDs analysis, which does not need to be limited only to the investigation of soil hydraulic properties. For example, potential applications can be also targeted to the optimization of the morphological characteristics of the LID itself (depth, slope, plants, etc) for a particular climate, to the optimization of the adsorption properties of filter layers, or for specific design aims. Such studies could help in providing a better understanding of LID techniques while promoting the widespread adoption of such systems.

Acknowledgements

References

Abbaspour, K.C., Schulin, R., van Genuchten, M.T., 2001. Estimating unsaturated soil hydraulic parameters using ant colony optimization. Adv. Water Resour. 24, 827–841. http://dx.doi.org/10.1016/S0309-1708(01)00018-5.

Abbaspour, K.C., Johnson, C.A., van Genuchten, M.T., 2004. Estimating Uncertain Flow and Transport Parameters Using a Sequential Uncertainty Fitting Procedure. Vadose Zo. J. 3, 1340–1352. http://dx.doi.org/10.2113/3.4.1340.

Abu-Zreig, M., Rudra, R.P., Whiteley, H.R., 2001. Validation of a vegetated filter strip model (VFSMOD). Hydrol. Process. 15, 729–742. http://dx.doi.org/10.1002/hyp.101.

Akat, S.B., Gazi, V., 2008. Particle swarm optimization with dynamic neighborhood topology: Three neighborhood strategies and preliminary results. In: 2008 IEEE Swarm Intelligence Symposium. pp. 1–8. http://dx.doi.org/10.1109/SIS.2008.4668298.

Allen, R.G., Pereira, L.S., Raes, D., Smith, M., 1998. FAO Irrigation and Drainage Paper No. 56: Crop Evapotranspiration. FAO, Rome.

Archer, G.E.B., Saltelli, A., Sobol, I.M., 1997. Sensitivity measures, anova-like Techniques and the use of bootstrap. J. Stat. Comput. Simul. 58, 99–120. http://dx.doi.org/10.1080/00949659708811825.

Bengtsson, L., Grahn, L., Olsson, J., 2004. Hydrological function of a thin extensive green roof in southern Sweden. Nord. Hydrol. 36, 259–268.

Berardi, U., GhaffarianHoseini, A., GhaffarianHoseini, A., 2014. State-of-the-art analysis of the environmental benefits of green roofs. Appl. Energy 115, 411–428. http://dx.doi.org/10.1016/j.apenergy.2013.10.047.

Blanusa, T., Vaz Monteiro, M.M., Fantozzi, F., Vysini, E., Li, Y., Cameron, R.W.F., 2013. Alternatives to sedum on green roofs: can broad leaf perennial plants offer better "cooling service"? Build. Environ. 59, 99–106. http://dx.doi.org/10.1016/j.buildenv.2012.08.011.

Borgonovo, E., Castaings, W., Tarantola, S., 2012. Model emulation and moment-independent sensitivity analysis: an application to environmental modelling. Environ. Model. Softw. 34, 105–115. http://dx.doi.org/10.1016/j.envsoft.2011.06.006.

Brattebo, B.O., Booth, D.B., 2003. Long-term stormwater quantity and quality performance of permeable pavement systems. Water Res. 37, 4369–4376. http://dx.doi.org/10.1016/S0043-1354(03)00410-X.

Breshears, D.D., Rich, P.M., Barnes, F.J., Campbell, K., 1997. Overstory-imposed heterogeneity in solar radiation and soil moisture in a semiarid woodland. Ecol. Appl. 7, 1201–1215. http://dx.doi.org/10.1890/1051-0761(1997) 007[1201: OIHISR]2.0.CO;2.

Brunetti, G., Simunek, J., Piro, P., 2016a. A comprehensive analysis of the variably-saturated hydraulic behavior of a green roof in a mediterranean climate. Vadose Zo. J. 15. http://dx.doi.org/10.2136/vzj2016.04.0032. In press.

Brunetti, G., Simunek, J., Piro, P., 2016b. A comprehensive numerical analysis of the hydraulic behavior of permeable pavement. J. Hydrol. 540, 1146–1161. doi: 10.2136/vzj2016.04.0032.

Brynjarsdottir, J., O'Hagan, A., 2014. Learning about physical parameters: the importance of model discrepancy. Inverse Probl. 30, 114007. http://dx.doi.org/10.1088/0266-5611/30/11/114007.

Carbone, M., Brunetti, G., Piro, P., 2014. Hydrological Performance of a Permeable Pavement in Mediterranean Climate. In: 14th SGEM GeoConference on Water Resources. Forest, Marine and Ocean Ecosystems. pp. 381–388. http://dx.doi.org/10.5593/SGEM2014/B31/S12.050.

Cey, E., Rudolph, D., Therrien, R., 2006. Simulation of groundwater recharge dynamics in partially saturated fractured soils incorporating spatially variable fracture apertures. Water Resour. Res. 42. http://dx.doi.org/10.1029/2005WR004589.

Cheviron, B., Coquet, Y., 2009. Sensitivity analysis of transient-MIM HYDRUS-1D: case study related to pesticide fate in soils. Vadose Zo. J. 8, 1064. http://dx.doi.org/10.2136/vzj2009.0023.

Coffman, L.S., 2002. Low-impact development: an alternative stormwater management technology. In: France, R.L. (Ed.), Handbook of Water Sensitive Planning and Design. Lewis Publishers Inc., pp. 97–123.

Collins, K.A., Hunt, W.F., Hathaway, J.M., 2008. Hydrologic comparison of four types of permeable pavement and standard asphalt in eastern north Carolina. J. Hydrol. Eng. 13, 1146–1157. http://dx.doi.org/10.1061/(ASCE)1084-0699(2008) 13:12(1146).

Dosskey, M.G., Helmers, M.J., Eisenhauer, D.E., Franti, T.G., Hoagland, K.D., 2002. Assessment of concentrated flow through riparian buffers. J. Soil Water Conserv. 57, 336–343. VL - 57.

Duan, Q., Sorooshian, S., Gupta, V., 1992. Effective and efficient global optimization for conceptual rainfall-runoff models. Water Resour. Res. 28, 1015–1031. http://dx.doi.org/10.1029/91WR02985.

Efron, B., Tibshirani, R., 1986. Bootstrap methods for standard errors, confidence intervals, and other measures of statistical accuracy. Stat. Sci. 1, 54–75.

Elliot, A., Trowsdale, S., 2007. A review of models for low impact urban stormwater drainage. Environ. Model. Softw. 22, 394–405. http://dx.doi.org/10.1016/j.envsoft.2005.12.005.

Fassman, E.A., Blackbourn, S., 2010. Urban runoff mitigation by a permeable pavement system over impermeable soils. J. Hydrol. Eng. 15, 475–485. http://dx.doi.org/10.1061/(ASCE)HE.1943-5584.0000238.

Feddes, R.A., Kowalik, P.J., Zaradny, H., 1978. Simulation of Field Water Use and Crop Yield. PUDOC, Wageningen.

Forrester, A.I.J., Sóbester, A., Keane, A.J., 2008. Engineering Design via Surrogate Modelling: A practical Guide. J. Wiley. http://dx.doi.org/10.1002/9780470770801.

Geiger, S., Cortis, A., Birkholzer, J.T., 2010. Upscaling solute transport in naturally fractured porous media with the continuous time random walk method. Water Resour. Res. 46. http://dx.doi.org/10.1029/2010WR009133. n/a–n/a.

Getter, K.L., Rowe, D.B., Andresen, J.A., 2007. Quantifying the effect of slope on extensive green roof stormwater retention. Ecol. Eng. 31, 225–231. http://dx.doi.org/10.1016/j.ecoleng.2007.06.004.

UMS GmbH, 2015. UMS (2015): Manual HYPROP, Version 2015-01.

Gutmann, H.M., 2001. A radial basis function method for global optimization. J. Glob. Optim. 19, 201–227. http://dx.doi.org/10.1023/A:1011255519438.

Hopmans, J.W., Šimůnek, J., Romano, N., Durner, W., 2002. Inverse modeling of transient water flow. In: Dane, J.H., Topp, G.C. (Eds.), Methods of Soil Analysis, Part 4, Physical Methods. SSSA, Madison, WI, pp. 963–1008.

Houska, T., Multsch, S., Kraft, P., Frede, H.-G., Breuer, L., 2013. Monte Carlo based calibration and uncertainty analysis of a coupled plant growth and hydrological model. Biogeosci. Discuss. 10, 19509–19540. http://dx.doi.org/10.5194/bgd-10-19509-2013.

Hu, S., 1987. Akaike information criterion statistics. Math. Comput. Simul. 29, 452. http://dx.doi.org/10.1016/0378-4754(87)90094-2.

Ines, A.V.M., Droogers, P., 2002. Inverse modelling in estimating soil hydraulic functions: a genetic algorithm approach. Hydrol. Earth Syst. Sci. Discuss. 6, 49–66.

Jones, D.R., 2001. A taxonomy of global optimization methods based on response surfaces. J. Glob. Optim. 21, 345–383. http://dx.doi.org/10.1023/A:1012771025575.

Jones, D.R., Schonlau, M., William, J., 1998. Efficient global optimization of expensive black-box functions. J. Glob. Optim. 13, 455–492. http://dx.doi.org/10.1023/a:1008306431147.

Keating, E.H., Doherty, J., Vrugt, J.A., Kang, Q., 2010. Optimization and uncertainty assessment of strongly nonlinear groundwater models with high parameter dimensionality. Water Resour. Res. 46. http://dx.doi.org/10.1029/2009WR8584. n/a-n/a.

Kennedy, J., Eberhart, R., 1995. Particle swarm optimization. Eng. Technol., 1942–1948

Kennedy, J., O'Hagan, A., 2001. Bayesian calibration of computer models. J. R. Stat. Soc. Ser. B (Statistical Methodol), 425–464. http://dx.doi.org/10.1111/1467-9868.00294.

Kennedy, J., Spears, W.M., 1998. Matching algorithms to problems: an experimental test of the particle swarm and some genetic algorithms on the multimodal problem generator. In: 1998 IEEE International Conference on Evolutionary Computation Proceedings. IEEE World Congress on Computational Intelligence (Cat. No.98TH8360). IEEE, pp. 78–83. http://dx.doi.org/10.1109/ICEC.1998.699326.

Khu, S.-T., Werner, M.G.F., 2003. Reduction of Monte-Carlo simulation runs for uncertainty estimation in hydrological modelling. Hydrol. Earth Syst. Sci. 7, 680–692. http://dx.doi.org/10.5194/hess-7-680-2003.

Laloy, E., Rogiers, B., Vrugt, J.A., Mallants, D., Jacques, D., 2013. Efficient posterior exploration of a high-dimensional groundwater model from two-stage Markov chain Monte Carlo simulation and polynomial chaos expansion. Water Resour. Res. 49, 2664–2682. http://dx.doi.org/10.1002/wrcr.20226.

Li, Y., Babcock, R.W., 2014. Green roof hydrologic performance and modeling: a review. Water Sci. Technol. 69, 727–738. http://dx.doi.org/10.2166/wst.2013.770.

Li, Y., Babcock, R.W., 2015. Modeling hydrologic performance of a green roof system with HYDRUS-2D. J. Environ. Eng. 141, 04015036. http://dx.doi.org/10.1061/(ASCE)EE.1943-7870.0000976.

Liang, J.J., Qin, A.K., Suganthan, P.N., Baskar, S., 2006. Comprehensive learning particle swarm optimizer for global optimization of multimodal functions. IEEE Trans. Evol. Comput. 10, 281–295. http://dx.doi.org/10.1109/TEVC.2005.857610.

Mackay, D.J.C., 1998. Introduction to Gaussian processes. Neural Networks Mach. Learn. 168, 133–165. http://dx.doi.org/10.1007/s10067-003-0742-1.

Marquardt, D.W., 1963. An algorithm for least-squares estimation of nonlinear parameters. J. Soc. Ind. Appl. Math. 11, 431–441. http://dx.doi.org/10.1137/0111030.

McKay, M.D., Beckman, R.J., Conover, W.J., 1979. Comparison of three methods for selecting values of input variables in the analysis of output from a computer code. Technometrics 21, 239–245. http://dx.doi.org/10.1080/00401706.1979.10489755.

Metselaar, K., 2012. Water retention and evapotranspiration of green roofs and possible natural vegetation types. Resour. Conserv. Recycl. 64, 49–55. http://dx.doi.org/10.1016/j.resconrec.2011.12.009.

Moriasi, D.N., Arnold, J.G., Van Liew, M.W., Binger, R.L., Harmel, R.D., Veith, T.L., 2007. Model evaluation guidelines for systematic quantification of accuracy in watershed simulations. Trans. ASABE 50, 885–900. http://dx.doi.org/10.13031/2013.23153.

Munoz-Carpena, R., Parsons, J.E., 2004. A design procedure for vegetative filter strips using VFSMOD-W. Trans. Asae 47, 1933–1941.

Nash, J.E., Sutcliffe, J.V., 1970. River flow forecasting through conceptual models: Part I – a discussion of principles. J. Hydrol. 10, 282–290. http://dx.doi.org/10.1016/0022-1694(70)90255-6.

Newcomer, M.E., Gurdak, J.J., Sklar, L.S., Nanus, L., 2014. Urban recharge beneath low impact development and effects of climate variability and change. Water Resour. Res. 50, 1716–1734. http://dx.doi.org/10.1002/2013WR014282.

Nossent, J., Elsen, P., Bauwens, W., 2011. Sobol' sensitivity analysis of a complex environmental model. Environ. Model. Softw. 26, 1515–1525. http://dx.doi.org/10.1016/j.envsoft.2011.08.010.

O'Hagan, A., 2006. Bayesian analysis of computer code outputs: a tutorial. Reliab. Eng. Syst. Saf. 91, 1290–1300. http://dx.doi.org/10.1016/j.ress.2005.11.025.

Oakley, J.E., O'Hagan, A., 2004. Probabilistic sensitivity analysis of complex models: a Bayesian approach. J. R. Stat. Soc. Ser. B Stat. Methodol. 66, 751–769. http://dx.doi.org/10.1111/j.1467-9868.2004.05304.x.

OECD, 2013. Water and climate change adaptation: policies to navigate uncharted waters. OECD Studies on Water. OECD Publishing, Paris. 10.1787/9789264200449-en.

Pan, L., Wu, L., 1998. A hybrid global optimization method for inverse estimation of hydraulic parameters: annealing-simplex method. Water Resour. Res. 34, 2261–2269. http://dx.doi.org/10.1029/98WR01672.

Pedersen, M.E.H., 2010. Good parameters for particle swarm optimization, Technical Report HL1001, Hvass Laboratories.

Pertassek, T., Peters, A., Durner, W., 2015. HYPROP-FIT Software User's Manual, V. 3.0.

Peters, A., Durner, W., 2008. Simplified evaporation method for determining soil hydraulic properties. J. Hydrol. 356, 147–162. http://dx.doi.org/10.1016/j.jhydrol.2008.04.016.

Python Software Foundation, 2013. Python Language Reference, version 2.7. Python Softw. Found.

Rasmussen, C.E., Williams, C.K.I., 2006. Gaussian Processes for Machine Learning. MIT Press, Cambridge, MA.

Razavi, S., Tolson, B.A., Burn, D.H., 2012. Review of surrogate modeling in water resources. Water Resour. Res. 48. http://dx.doi.org/10.1029/2011WR011527. n/a–n/a.

Regis, R.G., Shoemaker, C.A., 2004. Local function approximation in evolutionary algorithms for the optimization of costly functions. IEEE Trans. Evol. Comput. 8, 490–505. http://dx.doi.org/10.1109/TEVC.2004.835247.

Rezaei, M., Seuntjens, P., Joris, I., Boënne, W., Van Hoey, S., Campling, P., Cornelis, W. M., 2015. Sensitivity of water stress in a two-layered sandy grassland soil to variations in groundwater depth and soil hydraulic parameters. Hydrol. Earth Syst. Sci. Discuss. 12, 6881–6920. http://dx.doi.org/10.5194/hessd-12-6881-2015.

Ritchie, J.T., 1972. Model for predicting evaporation from a row crop with incomplete cover. Water Resour. Res. 8, 1204–1213. http://dx.doi.org/10.1029/WR008i005p01204.

Sacks, J., Welch, W.J., Mitchell, T.J., Wynn, H.P., 1989. Design and analysis of computer experiments. Stat. Sci. 4, 409–435. doi:10.1214/ss/1177012413.

Saltelli, A., Annoni, P., 2010. How to avoid a perfunctory sensitivity analysis. Environ. Model. Softw. 25, 1508–1517. http://dx.doi.org/10.1016/j.envsoft.2010.04.012.

Saltelli, A., Tarantola, S., Saisana, M., Nardo, M., 2005. What is sensitivity analysis? In: II Convegno Della Rete Dei Nuclei Di Valutazione E Verifica, Napoli 26, 27 Gennaio 2005, Centro Congressi Università Federico II, Via Partenope 36.

Saltelli, A., Annoni, P., Azzini, I., Campolongo, F., Ratto, M., Tarantola, S., 2010. Variance based sensitivity analysis of model output. Design and estimator for the total sensitivity index. Comput. Phys. Commun. 181, 259–270. http://dx.doi.org/10.1016/j.cpc.2009.09.018.

Schindler, U., 1980. Ein Schnellverfahren zur Messung der Wasserleitfähigkeit im teilgesättigten Boden an Stechzylinderproben. Arch. für Acker- und Pflanzenbau und Bodenkd. 24, 1–7.

Schindler, U., Durner, W., von Unold, G., Mueller, L., Wieland, R., 2010a. The evaporation method: extending the measurement range of soil hydraulic properties using the air-entry pressure of the ceramic cup. J. Plant Nutr. Soil Sci. 173, 563–572. http://dx.doi.org/10.1002/jpln.200900201.

Schindler, U., Durner, W., von Unold, G., Muller, L., 2010b. Evaporation method for measuring unsaturated hydraulic properties of soils: extending the measurement range. Soil Sci. Soc. Am. J. 74, 1071–1083. http://dx.doi.org/10.2136/sssaj2008.0358.

Schonlau, M., 1997. Computer experiments and global optimization (PhD thesis). University of Waterloo, Waterloo, Canada.

Sevat, E., Dezetter, A., Servat, E., 1991. Selection of calibration objective functions in the context of rainfall-runoff modelling in a sudanese savannah area. Hydrol. Sci. J. Des. Sci Hydrol. 36, 307–330. http://dx.doi.org/10.1080/02626669109492517.

Shi, Y., Eberhart, R., 1998. A modified particle swarm optimizer. In: 1998 IEEE Int. Conf. Evol. Comput. Proceedings. IEEE World Congr. Comput. Intell. (Cat. No.98TH8360), pp.69–73. http://dx.doi.org/10.1109/ICEC.1998.699146.

Shi, Y., Eberhart, R.C., 1999. Empirical study of particle swarm optimization. In: Proc. 1999 Congr. Evol. Comput. pp. 1945–1950. http://dx.doi.org/10.1109/CEC.1999.785511.

Šimůnek, J., van Genuchten, M.T., Šejna, M., 2008. Development and applications of the HYDRUS and STANMOD software packages and related codes. Vadose Zo. J. 7, 587. http://dx.doi.org/10.2136/vzj2007.0077.

Šimůnek, J., van Genuchten, M.T., Šejna, M., 2016. Recent DEVELOPMENTS and applications of the HYDRUS computer software packages. Vadose Zo. J. 15, 25. http://dx.doi.org/10.2136/vzj2016.04.0033.

Sobol', I., 2001. Global sensitivity indices for nonlinear mathematical models and their Monte Carlo estimates. Math. Comput. Simul. 55, 271–280. http://dx.doi.org/10.1016/S0378-4754(00)00270-6.

Sutanto, S.J., Wenninger, J., Coenders-Gerrits, A.M.J., Uhlenbrook, S., 2012. Partitioning of evaporation into transpiration, soil evaporation and interception: a comparison between isotope measurements and a HYDRUS-1D model. Hydrol. Earth Syst. Sci. 16, 2605–2616. http://dx.doi.org/10.5194/hess-16-2605-2012.

Taylor, S.A., Ashcroft, G.L., 1972. Physical Edaphology: The Physics of Irrigated and Nonirrigated Soils. Freeman, San Francisco, W.H.

Tokunaga, T.K., 2009. Hydraulic properties of adsorbed water films in unsaturated porous media. Water Resour. Res. 45, 1287–1295. http://dx.doi.org/10.1029/2009WR007734.

van Dam, J.C., Groenendijk, P., Hendriks, R.F.A., Kroes, J.G., 2008. Advances of Modeling Water Flow in Variably Saturated Soils with SWAP. Vadose Zo. J. 7, 640. http://dx.doi.org/10.2136/vzj2007.0060.

van Genuchten, M.T., 1980. A Closed-form Equation for Predicting the Hydraulic Conductivity of Unsaturated Soils1. Soil Sci. Soc. Am. J. 44, 892–898. http://dx.doi.org/10.2136/sssaj1980.03615995004400050002x.

Vrugt, J.A., Gupta, H.V., Bouten, W., Sorooshian, S., 2003. A Shuffled Complex Evolution Metropolis algorithm for optimization and uncertainty assessment of hydrologic model parameters. Water Resour. Res. 39. http://dx.doi.org/10.1029/2002WR001642. n/a–n/a.

Vrugt, J.A., Schoups, G., Hopmans, J.W., Young, C., Wallender, W.W., Harter, T., Bouten, W., 2004. Inverse modeling of large-scale spatially distributed vadose zone properties using global optimization. Water Resour. Res. 40. http://dx.doi.org/10.1029/2003WR002706. n/a–n/a.

Vrugt, J.A., Stauffer, P.H., Wöhling, T., Robinson, B.A., Vesselinov, V.V., 2008. Inverse modeling of subsurface flow and transport properties: a review with new developments. Vadose Zo. J. 7, 843. http://dx.doi.org/10.2136/vzj2007.0078.

Wang, G.G., Shan, S., 2007. Review of metamodeling techniques in support of engineering design optimization. J. Mech. Des. 129, 370. http://dx.doi.org/10.1115/1.2429697.

Wesseling, J., Elbers, J., Kabat, P., Broek, B. Van den, 1991. SWATRE: instructions for input. Intern. Note, Winand Star. Cent.

Wong, T.H.F., Fletcher, T.D., Duncan, H.P., Jenkins, G.A., 2006. Modelling urban stormwater treatment-A unified approach. Ecol. Eng. 27, 58–70. http://dx.doi.org/10.1016/j.ecoleng.2005.10.014.

Ye, K.Q., Li, W., Sudjianto, A., 2000. Algorithmic construction of optimal symmetric Latin hypercube designs. J. Stat. Plan. Inference 90, 145–159. http://dx.doi.org/10.1016/S0378-3758(00)00105-1.

Younes, A., Mara, T.A., Fajraoui, N., Lehmann, F., Belfort, B., Beydoun, H., 2013. Use of global sensitivity analysis to help assess unsaturated soil hydraulic parameters. Vadose Zo. J. 12. http://dx.doi.org/10.2136/vzj2011.0150.

Zhang, X., Srinivasan, R., Van Liew, M., 2009. Approximating SWAT Model using artificial neural network and support vector machine. JAWRA J. Am. Water Resour. Assoc. 45, 460–474. http://dx.doi.org/10.1111/j.1752-1688.2009.00302.x.